Check for updates

ChemistrySelect

Research Article
doi.org/10.1002/slct.202502538

Chemistry Europe
European Chemical Societies Publishing

www.chemistryselect.org

Determination of the Critical CTAB Concentration for the Carbon-supported CoB Catalysts Synthesis Toward Hydrogen Generation from $NABH_4$

Jülide Hazal Özdemir,*[a] Barış Aktaş,[a] Ayşegül Şirin,[a] and Oğuz Kaan Özdemir[a]

Hydrogen production from sodium borohydride ($NaBH_4$) is an inherently slow reaction, necessitating a catalyst to accelerate the process by lowering the activation energy. Cobalt (Co)-based catalysts have gained significant attention due to their affordability and high catalytic performance. However, despite their superior activity, agglomeration can hinder the catalytic efficiency of Co-based materials during reduction, attributed to their high surface energy and magnetic properties, ultimately leading to a lower hydrogen generation rate (HGR). In this study, the effect of cyclohexyl trimethyl ammonium bromide (CTAB), a cationic surfactant, in promoting the homogeneous dispersion of cobalt-boride (CoB) on a carbon support was investigated, and the critical CTAB concentration for the synthesis of carbon-supported CoB toward hydrogen generation from $NaBH_4$ was determined. Comprehensive characterization was performed, including HGR measurements, kinetic analysis, reusability and durability assessments, and physical characterization techniques. The results demonstrate that the addition of CTAB up to an optimal concentration (100 µL) enhances the HGR by approximately 70%, while exceeding this critical amount adversely affects and decreases the rate. Notably, the highest HGR achieved for the CoB/C-100CTAB catalyst was 37.34 ($L_{H2}/min*g_{catalyst}$), and the resultant activation energy for the reaction was determined to be 56 ($kJ*mol^{-1}$).

1. Introduction

The increasing environmental outcomes of non-renewable fossil fuels, including global warming and ecological degradation through pollution and greenhouse gas emissions, have emphasized the critical importance of developing eco-friendly and renewable alternative energy sources.[1] Among these alternatives, hydrogen is highly regarded as a clean energy carrier with significant potential, attributed to its superior combustion characteristics and high specific energy. Consequently, it is increasingly favored for applications ranging from internal combustion engines to fuel cells and is considered a key candidate to replace conventional petroleum-based resources. However, hydrogen is not a primary energy source but rather an energy carrier that necessitates production from various feedstocks using diverse methodologies, including biomass pyrolysis, water electrolysis, photocatalysis, and steam reforming of natural gas. Despite being one of the most abundant elements globally, hydrogen does not exist naturally in its diatomic form (H_2) and readily forms compounds, particularly hydrides, with other elements due to its reducing capabilities. Metal hydrides, formed through covalent bonding interactions between hydrogen atoms and central metal atoms (such as Li, La, Ti, Ni, V, Zr, and Fe), offer the advantage of high hydrogen storage capacities and enhanced safety profiles compared to traditional mechanical storage systems. Nevertheless, their widespread usage is currently hindered by limitations such as sluggish hydrogen absorption and desorption kinetics, sensitivity to impurities that can poison the material, insufficient reversibility over multiple cycles, and the requirement for relatively high temperatures to release the stored hydrogen effectively.[2,3]

Hydrogen storage remains a critical bottleneck in the practical deployment of hydrogen energy technologies. Among various strategies, chemical hydrogen storage systems have attracted growing attention due to their high volumetric hydrogen density, controllable release profiles, and potential for mild-condition operation. Representative hydrogen-rich media such as formic acid (HCOOH) and ammonia borane (NH_3BH_3) have been extensively investigated owing to their distinct dehydrogenation mechanisms and storage capacities. Formic acid, for example, offers high selectivity and low toxicity but suffers from relatively slow release kinetics and CO contamination in some catalytic systems.[4] On the other hand, ammonia borane possesses an exceptionally high gravimetric hydrogen content (~19.6 wt%) but presents challenges in regeneration and byproduct handling.[5] Chemical hydrides, including borohydrides (BH_4^-), alanates (AlH_4^-), and imides/amides (NH^-, NH_2^-), are attracting the interest of researchers for hydrogen storage and transportation due to their high hydrogen content, lower hydrolysis temperatures, and stability under ambient conditions. These properties are considered suitable for the requirements of economical and sustainable hydrogen storage.[6] Despite their general stability, chemical hydrides can be sensitive to oxygen and moisture, potentially resulting in the formation of toxic by-products that may adversely affect fuel cell performance. Moreover, slow adsorption/desorption kinetics often present a critical limitation in maintaining a continuous and effi-

[a] J. Hazal Özdemir, B. Aktaş, A. Şirin, O. Kaan Özdemir
Metallurgical and Materials Engineering, Yıldız Technical University, Istanbul, Turkey
E-mail: jhazal@yildiz.edu.tr

© 2025 Wiley-VCH GmbH

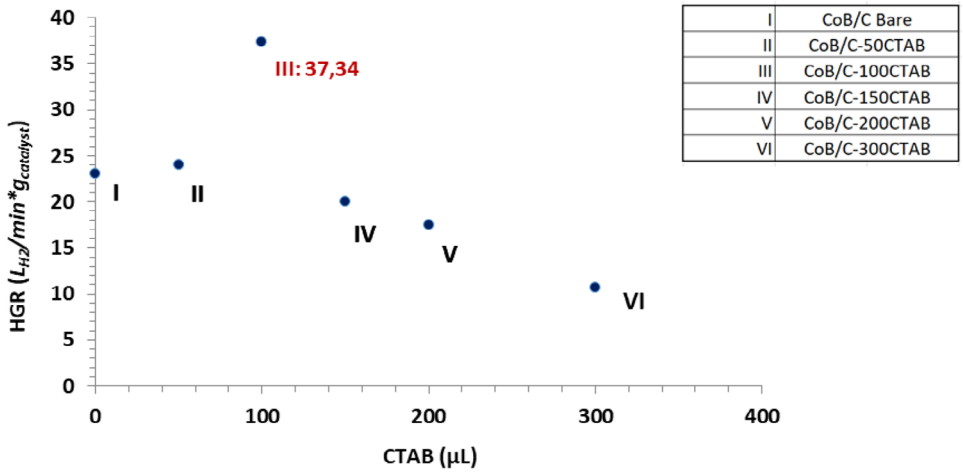


Figure 1. Calculated HGR values (L_{H2}/min*$g_{catalyst}$) for each catalyst material.

cient hydrogen supply.[7] For instance, alanates formed through the interaction of metal cations with AlH_4^- groups face several challenges, including production-related impurities, limited reversibility, lower hydrogen storage densities compared to other hydrides, and inherently slow reaction kinetics. These drawbacks restrict their practical application, particularly in the short term.[8] In contrast, boron- and nitrogen-containing hydrides, particularly borohydrides of alkali and alkaline earth metals (e.g., Na, Li, K, Be, Mg, Ca, Al, or NH_4), have emerged as highly promising candidates for hydrogen storage. These materials possess relatively high hydrogen content and form stable compounds where hydrogen is covalently bonded to boron atoms. Among their alternatives, borohydrides demonstrate superior gravimetric hydrogen storage capacities compared to alanates and imides/amides.[9,10] Notably, sodium borohydride ($NaBH_4$) offers additional advantages such as availability, ease of handling, higher functional group tolerance, stability, sustainable synthesis routes, relatively low cost, and a considerable gravimetric hydrogen storage density (10.8 wt %), making it critical for hydrogen storage studies.[11] The hydrogen storage-releasing reaction of $NaBH_4$ is given in Equation (1).

$$NaBH_4 + 2H_2O = NaBO_2 + 4H_2 + Heat \quad (1)$$

The right side of the hydrogen-releasing reaction from $NaBH_4$, often considered within a potentially reversible cycle for hydrogen storage, results in the generation of sodium metaborate ($NaBO_2$) as a by-product. The formation of hydrogen via the hydrolysis of $NaBH_4$ can be obtained under relatively lower temperatures (<80 °C).[12,13] Furthermore, the rate of hydrogen release and $NaBO_2$ formation can be regulated by changing the physical conditions, such as temperature, pressure, and the use of appropriate catalyst materials.[14,15] Therefore, as an emerging contender for fuel, especially for the proton exchange membrane fuel cells, the usage of $NaBH_4$ should be more deeply studied to determine appropriate concentrations, temperature/pressure conditions, and catalyst materials.

To catalyze the hydrolysis of $NaBH_4$, precious metals such as platinum (Pt), palladium (Pd), and ruthenium (Ru) demonstrate an excellent catalytic performance to obtain elevated-purity hydrogen from the reaction. However, the high costs of using noble metal catalysts prevent the widespread use of these precious metals. In this case, the need to investigate the catalytic effect of non-noble metals on the $NaBH_4$ hydrolysis reaction arises.[16] Within this framework, it has been observed that since these catalysts are cost-effective, have high catalytic performance, and adequate cycling stability, transition metals such as cobalt (Co), copper (Cu), nickel (Ni), and iron (Fe) or their complexes, particularly their metal borides, have gained attention among non-precious metal-based catalysts.[17] Cobalt-boride (CoB) catalysts have demonstrated sustained prominence in catalysis due to their enhanced catalytic activity, oxidation durability, and relatively low cost of production via facile chemical reduction. These factors have maintained their popularity from the past to the present.[18,19] The greater catalytic activity of the CoB catalyst is due to the electronic interaction between Co and B. The association of metalloid atoms (B or P) with transition metals such as Co, Fe, or Ni changes the internal electronic structure of the transition metals, which affects the catalytic performance. The regulation of electron dispersion around the centers subsequently makes the active Co sites more thermally and chemically stable.[20,21] The catalyst properties and composition are determinants for hydrogen generation from the hydrolysis of $NaBH_4$.[22] Although CoB materials show better performance, the agglomeration problem during reduction as a result of high surface energy and magnetic properties negatively affects their catalytic activity, and the final hydrogen generation rate is lower than expected.

Strategies to overcome this situation include alloying the CoB structure with other elements or using surface-active agents (ionic or non-ionic surfactants) that support the homogeneous distribution of catalysts. Surface-active agents have a unique structure with a polar, hydrophilic "head" and a non-polar, hydrophobic "tail." This amphipathic nature of these materials gives rise to their exceptional properties, such as solubility and surface activity.[23] Surfactants control the nucleation of catalysts during synthesis with their anionic and cationic units and aid the uniform distribution of catalyst particles on the carbon sup-

© 2025 Wiley-VCH GmbH

23656549, 2025, 30, Downloaded from https://chemistry-europe.onlinelibrary.wiley.com/doi/10.1002/slct.202502538 by Yildiz Teknik University, Wiley Online Library on [06/08/2025]. See the Terms and Conditions (https://onlinelibrary.wiley.com/terms-and-conditions) on Wiley Online Library for rules of use; OA articles are governed by the applicable Creative Commons License

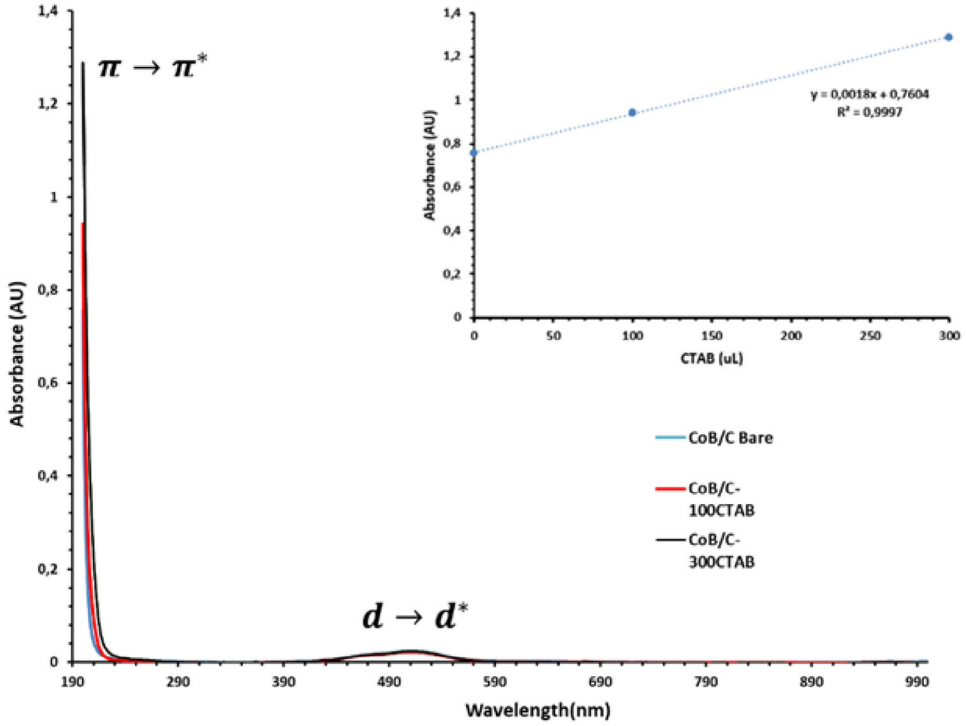


Figure 2. UV–vis absorption spectrum.

port material. By using surfactants, particle agglomeration due to steric effect and electrostatic repulsion is prevented.[24] Examples of well-known ionic/non-ionic surfactants are CTAB (cyclohexyl trimethyl ammonium bromide), SDS (sodium dodecyl sulfate), Tween (polysorbate 20), the Brij group, NP9 (nonylphenol ethoxylate), PVP (polyvinyl pyrrolidone), CTAC (cetyl trimethyl ammonium chloride), triton X-100 or SDBS (sodium dodecyl benzene sulfonate) that can be used to control the distribution of catalyst particles and carbon by creating an interface that will increase the dispersion of catalyst particles and provide suspension stability.[25] In a study performed by Kaya et al., the effect of Triton X-100 surfactant on CoB catalyst performance was investigated. The study showed that Triton included in the synthesis exhibited a higher HGR value (17.69 L_{H2}/min*$g_{catalyst}$) compared to the bare CoB catalyst (12.61 L_{H2}/min*$g_{catalyst}$).[26] In another study conducted by Loghmani et al., the effects of the PVP stabilization agent on the properties of the Co—La—Zr—B catalyst and hydrogen generation in the $NaBH_4$ hydrolysis reaction were investigated. Microscopy images show that PVP prevents the agglomeration of cubic nanoparticles. Furthermore, kinetic studies demonstrate that the required activation energy is lower compared to previous studies, representing a higher catalytic activity for the hydrolysis reaction.[27] Cetyl trimethyl ammonium bromide (CTAB), a cationic surfactant notable for its high affinity toward negatively charged surfaces, favorable aqueous solubility, and stability across a wide range of pH, is employed in the synthesis of various nanoparticles.[28] Its critical micelle concentration (CMC) is low compared to other surfactants (0.9 and 1.0 mM in water), which means that it can form effective micelles even at lower concentrations.[29] In a study performed by Chen et al., the effects of CTAB addition on copper nanowire-supported CoB catalyst for the ammonium borane hydrolysis reaction were investigated. The results show that CTAB-assisted copper nanowire support material aids homogeneous distribution for CoB, reduces the required activation energy by enhancing electron transfer, and creates a higher active site for ammonium borane hydrolysis reaction. These results are attributed to the high hydrophilic property of the CTAB that controls the morphology of the final catalyst.[30] In another study investigating the effects of CTAB surfactant addition on CoB catalyst properties, it was determined that the CoB catalyst synthesized with CTAB exhibited a higher surface area with 114.1 m^2/g, lower pore size with 12 nm, and a higher pore volume with 0.37 cm^3/g compared to CoB without CTAB incorporation, according to BET analysis results. Moreover, morphological examinations showed that while CoB without CTAB incorporation had an agglomerated spherical structure, a nanoflower structure with a greater surface area was obtained with the addition of CTAB. Gupta et al. prepared mesoporous Co—B nanocatalysts by the reduction of cobalt by $NaBH_4$ in the presence of CTAB surfactant, and concluded that Co-B/CTAB catalyst shows flower-like particles of the size in the range of 120–170 nm.[31] Loghmani et al. Cu—Fe—B catalysts were prepared by chemical reduction reaction, and they investigated the effect of polymers (PEG and PVP) and various surfactants (CTAB, SDS, and Triton X-100) as stabilizer agents on morphology and catalytic activity.[32] Baydaroglu et al. used the CTAB for directed chemical polymerization of polypyrrole.[33] Al-Thubaiti et al. have shown that CTAB and SDS were used to establish the effect of micelle head groups on the nucleation step of MnO_4 redox reactions with $NaBH_4$ and cysteine, and have proved that CTAB is a better surfactant than SDS for the synthesis of transition metal nanoparticles.[34]

© 2025 Wiley-VCH GmbH

23656549, 2025, 30, Downloaded from https://chemistry-europe.onlinelibrary.wiley.com/doi/10.1002/slct.202502538 by Yildiz Teknik University, Wiley Online Library on [06/08/2025]. See the Terms and Conditions (https://onlinelibrary.wiley.com/terms-and-conditions) on Wiley Online Library for rules of use; OA articles are governed by the applicable Creative Commons License

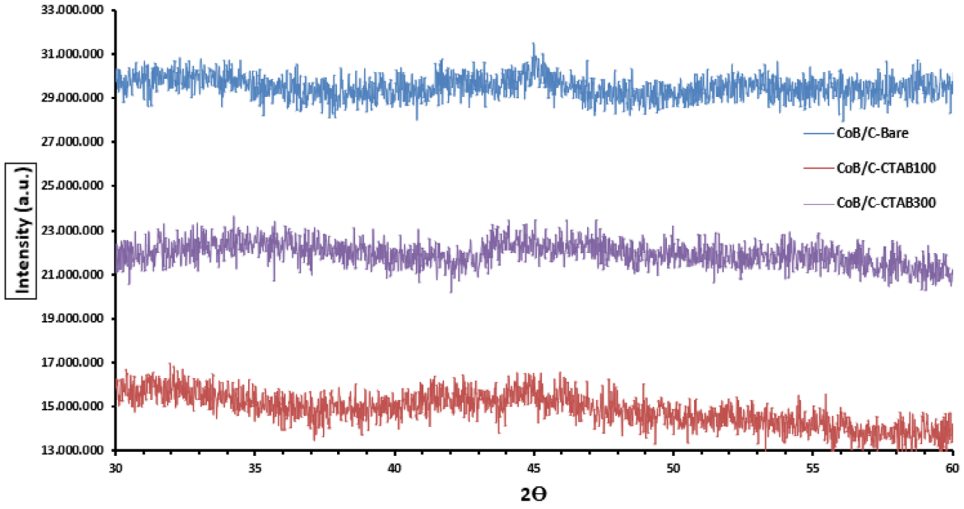


Figure 3. XRD patterns of carbon-supported CoB catalysts synthesized at different CTAB concentrations.

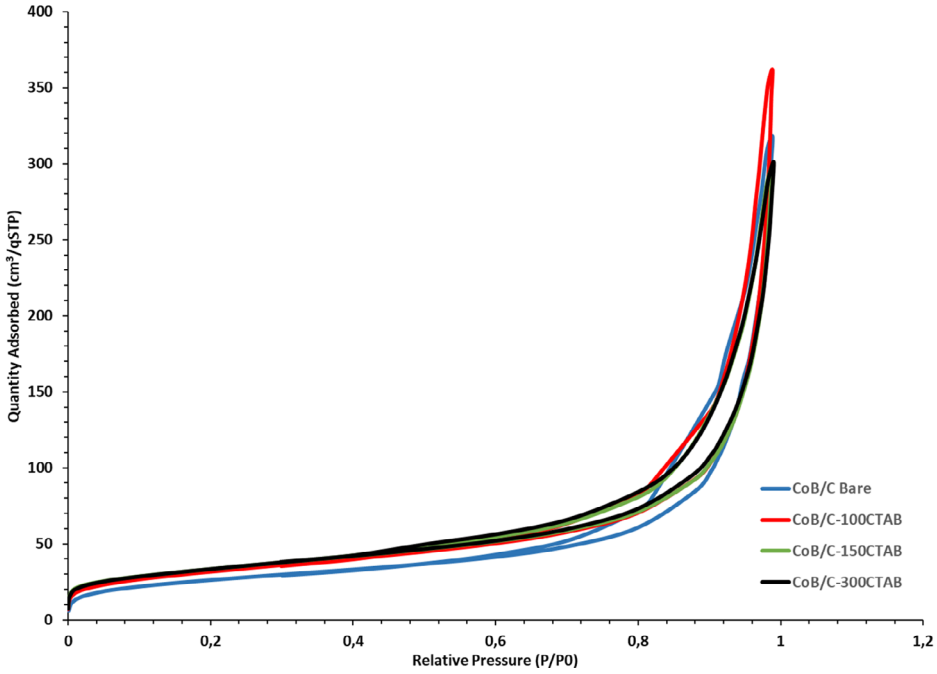


Figure 4. Adsorption/desorption isotherms of catalysts.

A review of the literature indicates that while the effects of CTAB in nanoparticle synthesis have been widely investigated, the determination of a critical concentration and its impact on catalytic performance remains insufficiently explored. Despite the knowledge of the positive effects of surface-active agents, our previous studies demonstrate that the amount of surfactant added to the synthesis adversely affects the catalyst performance after the optimum point. This publication aims to examine the effects of CTAB surfactant addition on carbon-supported CoB (CoB/C) catalyst synthesis from an experimental optimization perspective and reveal their effects on the $NaBH_4$ hydrolysis reaction. In this study, the impact of varying amounts of CTAB addition on the hydrolysis reaction of carbon-supported CoB catalysts with $NaBH_4$ was investigated. The optimum CTAB concentration for the synthesis of the catalyst with the highest hydrogen production rate was determined, and kinetic studies of this catalyst were carried out.

2. Materials and Methods

2.1. Catalysts Preparation

Catalysts were prepared using a chemical reduction method. Briefly, 28 mL of a 0.02 M $CoCl_2$ solution (97%, Sigma-Aldrich) was mixed with distilled water and 50 mg of carbon support (Vulcan XC-72), then ultrasonically dispersed for 30 min to ensure homogeneity. Based on our previously optimized CoB synthe-

© 2025 Wiley-VCH GmbH

23656549, 2025, 30, Downloaded from https://chemistry-europe.onlinelibrary.wiley.com/doi/10.1002/slct.202502538 by Yildiz Teknik University, Wiley Online Library on [06/08/2025]. See the Terms and Conditions (https://onlinelibrary.wiley.com/terms-and-conditions) on Wiley Online Library for rules of use; OA articles are governed by the applicable Creative Commons License

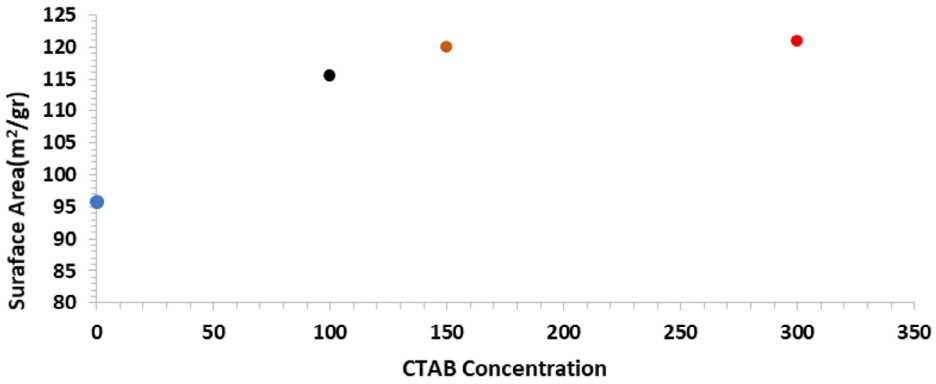


Figure 5. BET surface area changes as a function of CTAB concentration.

sis protocol, the reaction parameters were set as follows: pH 1 (adjusted using HCl, ACS reagent, Sigma–Aldrich), a reduction temperature of 5 °C, and a controlled addition rate of 5 mL min^{-1} for the reducing agent $NaBH_4$ (98%, Merck).[35] Following pH adjustment, the reaction beaker was placed in a 5 °C water bath. After the desired temperature was obtained, the reduction was initiated by adding a freshly prepared 10 mL $NaBH_4$ solution under continuous stirring at 500 rpm. A catalyst synthesized without CTAB (CoB/C) was used as the control group. To investigate the influence of the cationic surfactant CTAB (0.04 M in water), varying volumes (x = 50, 100, 150, 200, and 300 µL) were introduced during synthesis, yielding a series of CoB/C–xCTAB samples. All synthesized materials were washed by repeated centrifugation at 8000 rpm for 10 min, with intermediate mixing between each centrifugation using an orbital shaker. Only distilled water was used as the washing medium. Finally, the CoB/C–xCTAB samples were dried in a vacuum oven at 105 °C for 3 h.

2.2. Physical Characterization of Catalysts

The physical characterization of the synthesized CoB/C-based catalysts, prepared with and without the CTAB surfactant, was conducted using X-ray diffraction (XRD) and UV–vis spectroscopy (UV–vis). XRD patterns were recorded using Cu K_α radiation (λ = 1.54 Å) at 45 kV and 40 mA to identify the crystalline phases and assess the amorphous structure of the CoB/C-based materials. The specific surface area and porosity of the catalysts were determined by Brunauer–Emmett–Teller (BET) analysis. Additionally, the surface morphologies of the catalysts were examined using Field emission scanning electron microscopy (FE-SEM) at varying magnifications. These comprehensive analyses provided insights into the influence of the CTAB surfactant on the physical properties of the CoB/C–xCTAB catalysts during synthesis.

2.3. Determination of Hydrogen Generation Rate (HGR, $L_{H2}/min*g_{catalyst}$)

The water displacement method was used to determine the HGR values of the $NaBH_4$ hydrolysis reaction of bare and CTAB-added CoB/C catalysts. In this context, the total hydrogen volume produced and total reaction time were determined, and the HGR values were calculated in terms of $L_{H2}/min*g_{catalyst}$ with the formula given in Equation (2).

$$\frac{\text{Total hydrogen volume (mL)}}{\text{Catalyst amount (mg)} \times \text{Total time (min)}} \quad (2)$$

The standard test procedure is as described below.[26] The system required for the test was provided by a water bath with a water displacement mechanism connected to an integrated magnetic stirring system. 17 mg of synthesized catalyst and $NaBH_4$ (5 wt %) and NaOH (5 wt %) (ACS reagent, >97%, pellets, Sigma–Aldrich), containing 10 mL of fuel, were transferred to a 250 mL reactor. The test temperature is 65 °C and 840 rpm stirring was applied to the catalyst-fuel mixture. The HGR value was calculated by recording the hydrogen volume (mL) released per min. Additionally, to investigate the effects of the $NaBH_4$ and NaOH concentrations constituting the fuel on HGR, tests were carried out using different fuel concentrations, and HGR data were evaluated in detail.

2.4. Kinetic Measurements

To investigate the catalytic activity of the CoB/C-based catalyst exhibiting the optimum performance and to determine the activation energy, kinetic studies were carried out at four different temperatures (65 °C, 55 °C, 45 °C, and 35 °C). In this study, measurements were carried out using 17 mg of catalyst material and fuel containing 5 (wt %) $NaBH_4$ and 5 (wt %) NaOH for each temperature, and the obtained HGR values were recorded. The reaction rates obtained from the experiments at different temperatures were evaluated using the Arrhenius equation given in Equation (3).

$$\ln k = \ln A - \frac{Ea}{R \times T} \quad (3)$$

An Arrhenius plot was constructed based on the linear relationship derived from this equation involving the rate constant (k), absolute temperature (T-Kelvin), frequency factor (A-constant), and universal gas constant (R). The activation energy

© 2025 Wiley-VCH GmbH

23656549, 2025, 30, Downloaded from https://chemistry-europe.onlinelibrary.wiley.com/doi/10.1002/slct.202502538 by Yildiz Teknik University, Wiley Online Library on [06/08/2025]. See the Terms and Conditions (https://onlinelibrary.wiley.com/terms-and-conditions) on Wiley Online Library for rules of use; OA articles are governed by the applicable Creative Commons License

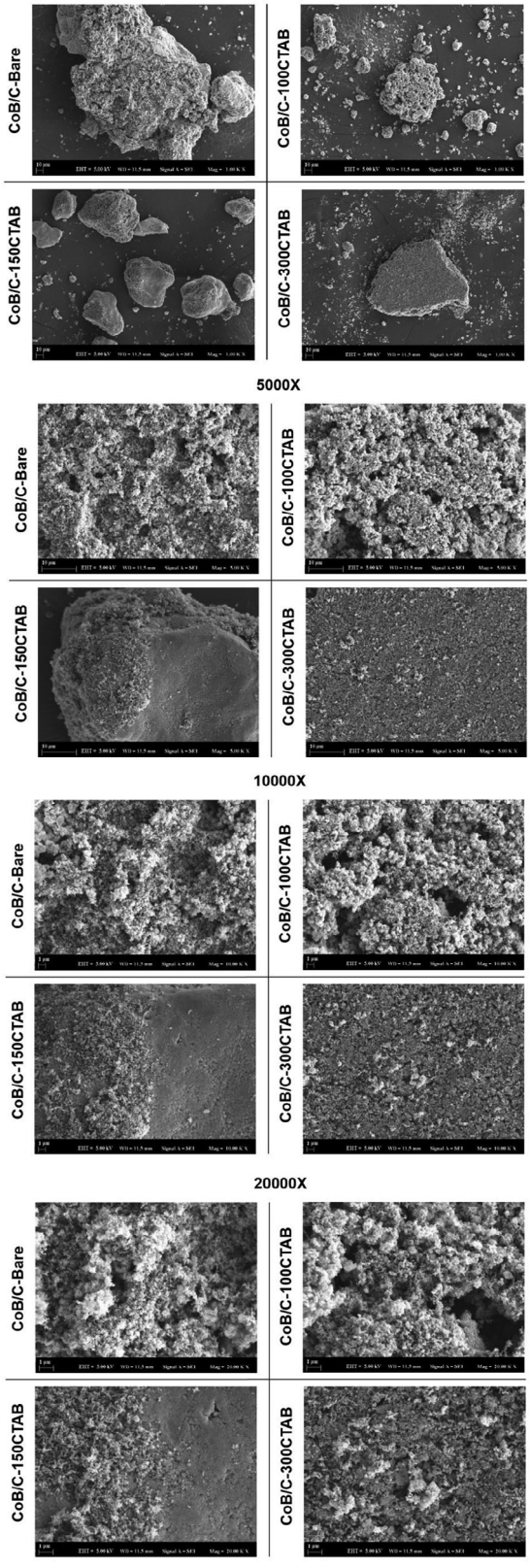


Figure 6. The FE-SEM images of the catalysts were taken at different magnifications.

of the catalyst was then calculated from the slope of the linear regression line.[36]

2.5. Reusability Testing of the Catalyst

To evaluate the reusability of the CoB/C-based catalysts in the NaBH4 hydrolysis reaction, 17 mg of the catalyst exhibiting optimal performance within this study was used to measure hydrogen generation rates (HGR) at a test temperature of 65 °C, employing a fuel solution of 5 (wt %) $NaBH_4$ and 5 (wt %) NaOH. After the completion of each hydrolysis reaction, the catalyst was recovered from the reaction medium and subjected to a washing procedure involving four cycles of centrifugation at 8000 rpm with distilled water, followed by drying in a vacuum oven at 0.25 bar and 105 °C for 3 h. The dried catalyst was then reused under identical test conditions, and this cycle was repeated five times to assess the catalyst's sustained activity. The fuel quantity for each subsequent cycle was adjusted proportionally to the remaining catalyst mass to account for catalyst loss during the washing steps.[37]

2.6. Durability Testing of the Catalyst

To assess the long-term operational stability of the catalysts, durability tests were conducted at a constant temperature of 65 °C. Approximately 17 mg of the desired catalyst was used with a fuel solution containing 5 (wt %) $NaBH_4$ and 5 (wt %) NaOH to measure the initial hydrogen generation rate (HGR). After the complete hydrolysis of $NaBH_4$ in the first cycle, a fresh 10 mL portion of the same fuel solution was added to the system to evaluate the catalyst's durability, and HGR values were recorded accordingly. These tests were continued for up to five cycles, as long as the catalyst maintained a noticeable level of activity.[38]

3. Results and Discussion

Surfactants, being amphiphilic molecules with both hydrophilic and hydrophobic properties, can form a variety of aggregates, including monomers, dimers, trimmers, and micelles, depending on their concentration.[34] When these molecules self-aggregate in water above the critical micelle concentration (CMC), they can form micelles and vesicles. The presence of surfactants affects the rate of various redox reactions through hydrophobic and electrostatic interactions. Micelles are stable in thermodynamic terms but can be kinetically unstable. The primary driving force behind the formation of these amphiphilic structures in water is the hydrophobic effect.[39] For this reason, there are certain concentration values at which the effect of surfactants on catalytic properties is highest, and this study aimed to determine the critical micelle concentration of CTAB surfactant for carbon-supported CoB catalyst. For this purpose, while preparing CoB catalysts by chemical reduction technique, CTAB was added to $CoCl_2$ solution at different concentrations, and the effect of

© 2025 Wiley-VCH GmbH

23656549, 2025, 30, Downloaded from https://chemistry-europe.onlinelibrary.wiley.com/doi/10.1002/slct.202502538 by Yildiz Teknik University, Wiley Online Library on [06/08/2025]. See the Terms and Conditions (https://onlinelibrary.wiley.com/terms-and-conditions) on Wiley Online Library for rules of use; OA articles are governed by the applicable Creative Commons License

the synthesized catalysts on the hydrolysis reaction is given in Figure 1.

As given in Figure 1, the addition of 50 µL of CTAB did not cause any significant change in the hydrogen production rate (HGR) of the catalyst. In contrast, the HGR of the catalyst increased by approximately 70% as a result of the addition of 100 µL of CTAB. The absence of a significant difference in HGR between the bare sample (CoB/C-Bare) and the one synthesized with 50 µL of CTAB (CoB/C-50CTAB) can primarily be attributed to the insufficient concentration of CTAB to reach its critical micelle concentration (CMC). As a cationic surfactant, CTAB must exceed the CMC level to form micellar structures capable of influencing nanoparticle morphology and surface properties effectively. At concentrations below this critic level, such as 50 µL, CTAB cannot promote notable reductions in particle size or guide the structural evolution of CoB. Furthermore, the adsorption of such a small amount of CTAB onto the CoB surface is likely insufficient to induce meaningful surface modification or stabilization. Additionally, the steric stabilization provided by this limited surfactant amount is inadequate to prevent particle agglomeration or enhance charge and ion transport pathways. In summary, a CTAB concentration as low as 50 µL does not allow for substantial micelle formation, morphological control, or electrochemical enhancement, which explains the lack of measurable improvement in HGR compared to the bare catalyst. As a result of the micelles formed by the addition of the optimum amount of surfactant, promoting the controlled growth of metal borides (100 µL added (CoB/C-100CTAB) sample for this study), CoB particles are well distributed on the surface, do not agglomerate, and more active areas are exposed for catalytic activity.[40,41]

However, it was interesting that further addition of CTAB caused a dramatic and gradual negative impact on HGRs from CoB/C-100CTAB catalyst (III) to CoB/C-300CTAB catalyst (VI). The effect of cationic surfactants such as CTAB on the synthesis of CoB catalysts and their HGR is governed by both physical and chemical interactions.[30] In the synthesis of cobalt boride (CoB) catalysts via sodium borohydride reduction, the usage of cationic surfactants such as CTAB significantly influences particle nucleation, growth mechanism, and dispersion stability. CTAB molecules adsorb electrostatically onto electron-rich regions of the growing CoB surface through their positively charged ammonium headgroups. The long hydrophobic alkyl tails extend outward, restricting crystal growth in certain directions and promoting the formation of uniform particles with higher surface area, which can enhance the catalytic performance during hydrogen generation reactions. At optimal concentrations, CTAB assists in producing well-dispersed nanoparticles by minimizing agglomeration and controlling the size distribution.[28] However, when used in excess, CTAB begins to inhibit catalytic activity. Surface over-coverage with surfactant molecules limits the accessibility of reactive BH_4^- ions to the Co active sites, and above the critical micelle concentration (CMC), CTAB micelles may isolate Co^{2+} ions, reducing their availability for nucleation and resulting in non-uniform growth and reduced catalytic surface area. Furthermore, increased steric hindrance on the surface may hinder proton access and gas diffusion, thereby lowering the hydrogen generation rate (HGR). These findings underscore the dual role of CTAB as both a morphological regulator and a potential kinetic barrier when used beyond optimal levels, highlighting the necessity of careful surfactant concentration optimization in catalyst design.[42]

In order to determine the effect of various CTAB concentrations on the catalytic activity of carbon-supported CoB, UV–vis absorption spectra (Figure 2) were obtained.

In the UV–vis spectrometer shown in Figure 2, two adsorption bands are observed for all catalysts. One of them is in the visible region, and the other is in the UV region. The absorption bands positioned in the visible region were due to the d-d transition, while the absorption bands located within the ultraviolet region were attributed to the ligand $\pi \rightarrow \pi^*$ transition and a blue shift likely from ligand-to-metal charge transition due to the restoration of electronic conjugation. Therefore, it can be concluded that CoB aggregates become smaller, efficiently separated, and distributed on carbon particles with the use of CTAB until an optimal amount. Thus, higher HGRs were obtained. Excessive amounts of surfactant usage caused irregular micelle formations, which resulted in greater micelles, bigger particles, lower catalytic activity, and lower HGR values. Additionally, the cationic surfactant proved effective in dispersing the Co nanoplatelets in water, likely due to its lower critical micellization concentration.

Figure 3 demonstrates the XRD patterns of carbon-supported CoB catalysts prepared with varying CTAB concentrations. No distinct peaks were observed in the XRD patterns of all carbon-supported CoB catalysts, suggesting that the CoB exhibited an amorphous structure when supported on carbon. This result is consistent with the literature.[43,44] The amorphous phase features a distinct structure characterized by short-range order and long-range disorder, along with unsaturated surface coordination sites, which can enhance catalytic activity for the hydrolysis of borohydride.[36]

The isothermal adsorption-desorption curves for the catalysts are given in Figure 4. The isotherms display a concave downward shape across the entire pressure range, suggesting that they correspond to the Type III isothermal classification.[26] Type III isotherms generally occur in systems where the adsorbate (such as gas molecules) has weak interactions with the surface of the adsorbent. This results in a curve where adsorption increases at low pressures but then decreases or levels off at higher pressures. This behavior is often seen with materials that do not have a strong binding affinity for the adsorbate, and the adsorbate molecules are typically more likely to form clusters or aggregates rather than strongly adhering to the surface.

The samples show the existence of both macropores and mesopores (evidenced by the steep increase in the adsorption isotherm above $P/P_0 = 0.9$ and the presence of the hysteresis loop). A wider hysteresis loop is seen in the relative pressure range of 0.40–0.99 for the CoB/C-100CTAB isotherm, suggesting it possesses a more porous structure. Figure 5 demonstrates the changes in the BET surface area of the synthesized catalysts with the amount of CTAB added. Accordingly, as the CTAB concentration increases, the BET surface area also increases, with the highest surface area obtained for the CoB/C-300CTAB catalyst.

© 2025 Wiley-VCH GmbH

23656549, 2025, 30, Downloaded from https://chemistry-europe.onlinelibrary.wiley.com/doi/10.1002/slct.202502538 by Yildiz Teknik University, Wiley Online Library on [06/08/2025]. See the Terms and Conditions (https://onlinelibrary.wiley.com/terms-and-conditions) on Wiley Online Library for rules of use; OA articles are governed by the applicable Creative Commons License

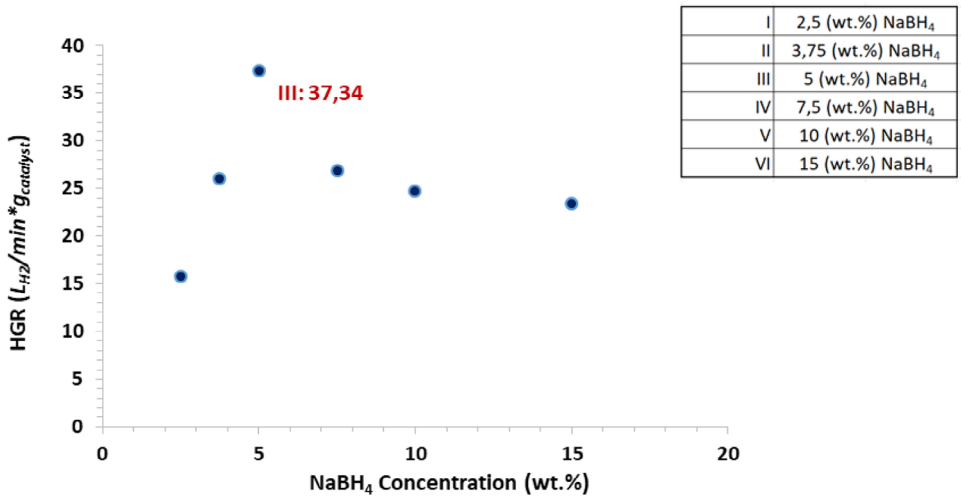


Figure 7. Comparison of HGR with different $NaBH_4$ concentrations for CoB/C-100CTAB catalyst.

Despite exhibiting the highest surface area according to BET analysis, the CoB/C-300CTAB sample exhibited relatively lower catalytic activity, which is a commonly encountered phenomenon in electrochemical systems. This inconsistency primarily arises from the fundamental difference between total physical surface area and the actual number of catalytically active sites. While BET analysis measures the entire accessible surface, including micro-, meso-, and macropores through gas adsorption, it does not distinguish whether these regions are catalytically functional.[45] In contrast, catalytic activity depends on the presence of surface sites that are both accessible to electrolyte ions and capable of facilitating electron transfer. If the material's porosity is dominated by micropores or obstructed regions, the restricted ion diffusion limits the number of sites effectively involved in catalytic reactions. Additionally, excessive use of surfactants such as CTAB can block surface sites or interfere with electron pathways, thereby reducing the material's overall catalytic efficiency even if the measured surface area remains high.[46]

Figure 6 presents FE-SEM images of the catalysts with various magnifications. As observed in the FE-SEM images, the addition of CTAB during synthesis leads to a significant reduction in particle size. With increasing CTAB concentration, the reduction in particle size continues, albeit to a lesser extent. This result corroborates the BET surface area findings. On the other hand, when the CTAB concentration exceeds 100 µL, the porosity in the catalyst structure significantly decreases, as evidenced by the adsorption/desorption hysteresis curve.

The kinetics of $NaBH_4$ hydrolysis catalyzed by carbon-supported CoB was examined concerning the initial concentrations of $NaBH_4$, NaOH, and temperature. The impact of $NaBH_4$ concentration on the rate of hydrogen generation was investigated by conducting a series of experiments with initial $NaBH_4$ concentrations ranging from 2.5 (wt %) to 15 (wt %). The comparison of HGRs (L_{H2}/min*$g_{catalyst}$) obtained is presented in Figure 7.

The hydrogen generation rate increases linearly with increasing $NaBH_4$ concentration from 2.5 (wt %) to 5 (wt %), and reaches a maximum of 37.34 L_{H2}/min*$g_{catalyst}$ for 5 (wt %) $NaBH_4$ solution. However, at concentrations higher than 5 (wt %) of $NaBH_4$, the hydrogen production rate first drops suddenly, and this decrease continues more slowly with increasing concentration values. A similar trend was observed by Kytsya and coworkers.[47] This result was attributed to higher $NaBH_4$ concentrations making the solution more viscous, preventing diffusion to the catalyst surface. Furthermore, because the by-product $NaBO_2$ is less soluble than $NaBH_4$, it may build up on the catalyst surface as the concentration of $NaBH_4$ increases. This case can be attributed to the rise in the "$NaBH_4$/catalyst" ratio, and it can also be concluded that the rate of the reaction is diffusion-controlled. Although the self-hydrolysis of $NaBH_4$ at room temperature is relatively slow, it can be entirely inhibited by using a highly basic solution. However, a high concentration of the stabilizing agent not only raises the solution pH but also slows the hydrolysis reaction rate. Thus, identifying an optimal NaOH concentration is crucial for maximizing the catalytic activity of the catalyst used. To investigate the effect of NaOH concentration on the hydrolysis of $NaBH_4$, the NaOH concentration was varied from 1 (wt %) to 15 (wt %) while maintaining a constant $NaBH_4$ concentration of 5 (wt %). Figure 8 gives the plot of the hydrogen generation rate as a function of different NaOH concentrations.

The hydrogen generation rate rises significantly when the NaOH concentration in the fuel solution is increased from 1 (wt %) to 5 (wt %), and HGR reached its maximum of 37.34 L_{H2}/min*$g_{catalyst}$. Upon further increase in NaOH concentration above 5 (wt %), a drastic decrease was observed. It seems that the hydroxyl ion functions in different mechanisms at low and high concentrations and probably has two different effects. First, the participation of OH^- ions in the catalytic reaction pathway of $NaBH_4$ hydrolysis. Therefore, HGR was boosted when the sodium hydroxide concentration was increased from 1 (wt %) to 5 (wt %). On the other hand, at higher NaOH concentrations, the solution pH rises, leading to an increase in OH^- ions, which inhibit the hydrolysis reaction and reduce proton concentration. This gradual ionization of $NaBH_4$ negatively impacts catalytic activity. When these two mechanisms are taken into account, the latter

© 2025 Wiley-VCH GmbH

23656549, 2025, 30, Downloaded from https://chemistry-europe.onlinelibrary.wiley.com/doi/10.1002/slct.202502538 by Yildiz Teknik University, Wiley Online Library on [06/08/2025]. See the Terms and Conditions (https://onlinelibrary.wiley.com/terms-and-conditions) on Wiley Online Library for rules of use; OA articles are governed by the applicable Creative Commons License

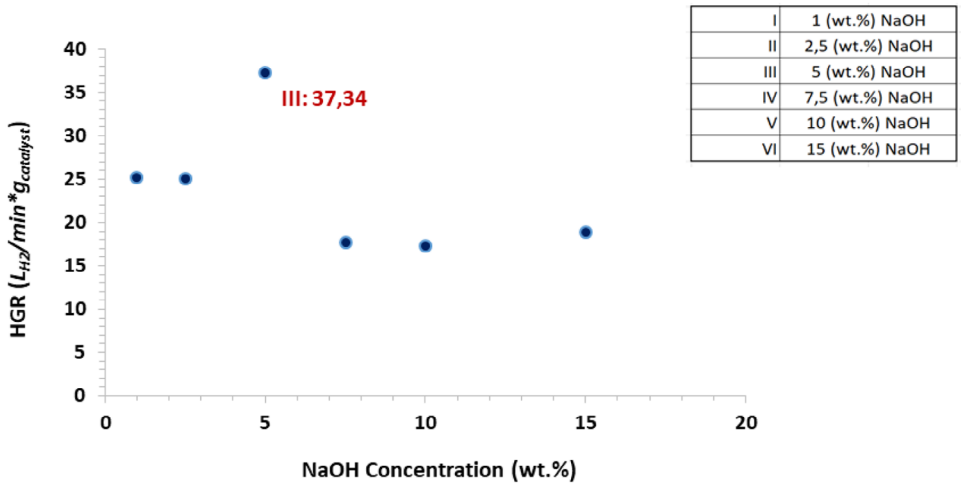


Figure 8. HGR values for the CoB/C-100CTAB catalyst with fuel having different NaOH concentrations.

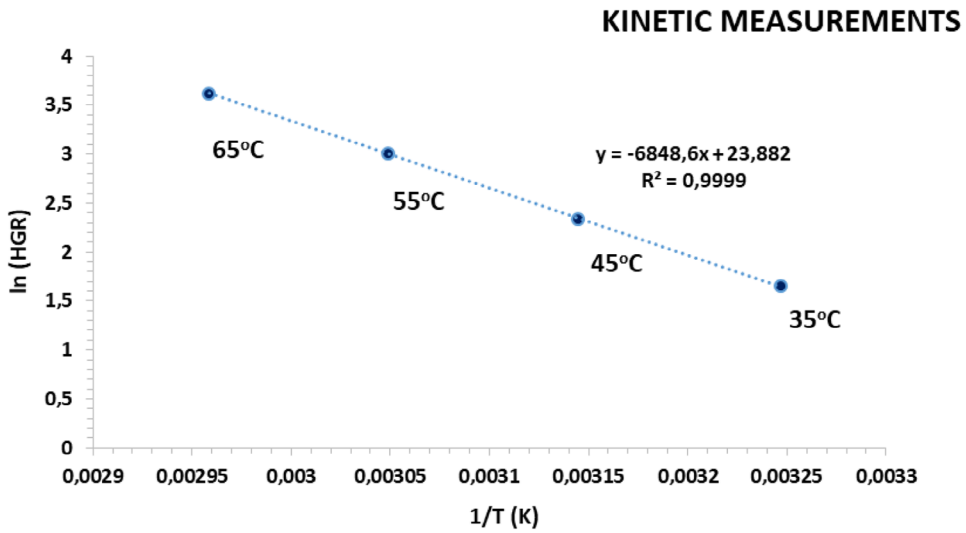


Figure 9. Arrhenius plot to determine the activation energy.

mechanism prevails when the NaOH concentration exceeds 5 (wt %).[48,49]

To assess the catalytic performances of CoB/C-100CTAB catalysts, the activation energy barrier was evaluated using an Arrhenius plot based on hydrogen generation yield measurements at various solution temperatures ranging from 35 °C to 65 °C, staring with the constant initial amounts of $NaBH_4$ (5 wt %), NaOH (5 wt %) and carbon-supported CoB catalyst (17 mg). Figure 6 shows the plot of the hydrogen generation rate versus temperature. It is evident that the hydrogen generation rate rises as the solution temperature increases from 35 °C to 65 °C. The slope of the Arrhenius plot reveals the activation energy of the hydrolysis reaction. The apparent activation energy (E_A) was measured as 56 kJ.mol^{-1}. In addition, as can be seen from Figure 9, the points belonging to different temperatures given in the Arrhenius curve coincide exactly on a line with a high correlation coefficient.

Table 1 represents a comparative summary of the activation energies determined for the catalytic hydrolysis of $NaBH_4$ using CoB/C–100CTAB (this study) and the other synthesized catalysts in the literature.

One of the key challenges in utilizing any catalyst in industry is ensuring that it is highly effective and can sustain its activity over time under the relevant operating conditions. A sequence of catalytic activity tests was carried out to evaluate the reusability of the CoB/C-100CTAB catalyst (Figure 10). Reusability tests were carried out under optimum conditions determined for the CoB/C-100CTAB catalyst. After each hydrolysis reaction, the used catalyst was taken from the reactor and carefully washed with pure water to remove the metaborates, which are the products of the hydrolysis reaction. After the washing process, the catalysts were left to dry in a vacuum environment at 105 °C for 3 h.

As can be seen in Figure 10, a linear decrease is observed between the HGR performance and the repeated use of catalysts. At the end of the 5th activity test, the HGR value of the catalyst shows an activity of approximately 58% of the initial performance. This reduction in catalytic activity can be attributed to

© 2025 Wiley-VCH GmbH

23656549, 2025, 30, Downloaded from https://chemistry-europe.onlinelibrary.wiley.com/doi/10.1002/slct.202502538 by Yildiz Teknik University, Wiley Online Library on [06/08/2025]. See the Terms and Conditions (https://onlinelibrary.wiley.com/terms-and-conditions) on Wiley Online Library for rules of use; OA articles are governed by the applicable Creative Commons License

23656549, 2025, 30, Downloaded from https://chemistry-europe.onlinelibrary.wiley.com/doi/10.1002/slct.202502538 by Yildiz Teknik University, Wiley Online Library on [06/08/2025]. See the Terms and Conditions (https://onlinelibrary.wiley.com/terms-and-conditions) on Wiley Online Library for rules of use; OA articles are governed by the applicable Creative Commons License

Table 1. Arrhenius activation energy for various catalyst systems used for the hydrolysis of sodium borohydride.

Catalyst	Reaction medium	E_A (kJ*mol^{-1})	Refs.
CoB/o-CNTs	0.5 g $NaBH_4$ + 1.875 g NaOH in 50 mL H_2O	37.63	[50]
CoB/C(30%)	0.2 M $NaBH_4$ + 0.02 M NaOH	44.43	[51]
Co-B/HPCM-2	5 wt % $NaBH_4$ + 2.25 wt % NaOH	43.30	[52]
Co-B/G	10 wt % $NaBH_4$ + 5 wt % NaOH	51.30	[53]
Co-B/CB	10 wt % $NaBH_4$ + 5 wt % NaOH	56.70	[13]
CoB/PANI NT	1 wt % $NaBH_4$ + 5 wt % NaOH	37.75	[54]
Co-B-50GO	5 wt % $NaBH_4$ + 5 wt % NaOH	26.20	[55]
CoB/TiO_2-x	0.04 g $NaBH_4$ + 0.04 g NaOH in 10 mL	57.03	[56]
CoB/Al_2O_3	1.0 wt % $NaBH_4$ + 3.75 wt % NaOH	56.80	[57]
Co–Mo–B/CC	5 wt % $NaBH_4$ + 7 wt % NaOH	51.00	[58]
Co–B/C	1.5 wt % $NaBH_4$ + 5.0 wt % NaOH	56.37	[59]
CoB/C-100CTAB	5 wt % $NaBH_4$ + 5 wt % NaOH	56.00	This study

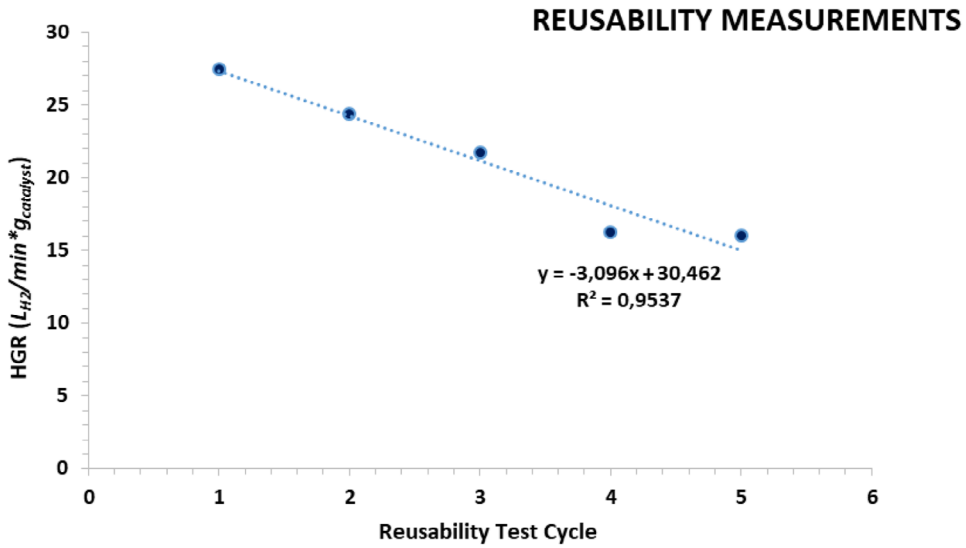


Figure 10. Hydrogen generation yield % in five sequential catalytic runs.

the deposition of trace amounts of sodium metaborate byproduct on the catalyst surface. In addition, surface oxidation of cobalt-based catalysts is another important factor that causes this decrease in catalytic activity.[59]

One of the significant challenges in the development of borohydride-proton exchange membrane fuel cells is the catalyst's susceptibility to deactivation.[60,61] Indeed, during operation, the catalyst is typically exposed to the ambient atmosphere, which can lead to deactivation. To assess the impact of this ambient condition on catalytic properties, CoB/C-100CTAB was exposed to the environment and tested at five intervals for its catalytic activity in the hydrolysis of alkaline $NaBH_4$ solution (Figure 11).

As given in Figure 11, a significant decrease in H_2 generation rate is observed for CoB/C-100CTAB powder after first usage: in that case, the hydrogen production rate of the catalyst decreased to almost 60% of the fresh powder rate. In the following repetitions, the HGR value continues to decrease linearly with the test cycle. The durability test curve given for the CoB/C-100CTAB catalyst shows a parabolic approach. Consequently, it is predicted that the hydrogen production rate of the catalysts will remain constant after a certain usage cycle. According to this parabolic approach, the surfaces of the catalysts are largely blocked by the metaborates released as reaction products as a result of the use of the first 10 mL of fuel, and a significant decrease in the performance of the catalyst occurs. This sharp decrease in the first test is thought to be due to the absorption of metaborates by the pores of the carbon support material due to capillary action, which results in slow diffusion of BH_4^- ions to the catalyst surface.

© 2025 Wiley-VCH GmbH

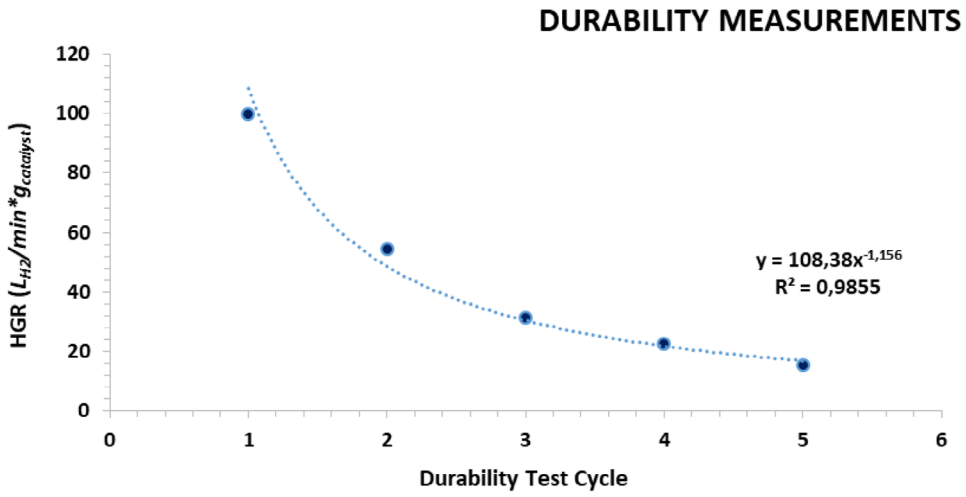


Figure 11. Percent of initial catalytic activity of CoB/C-100CTAB in successive runs after reuse for the hydrolysis of $NaBH_4$.

4. Conclusion

In this study, carbon-supported cobalt-boron (CoB) catalysts were synthesized via a chemical reduction method and employed in the hydrolysis of alkaline sodium borohydride ($NaBH_4$) solutions. This research investigated how the concentration of CTAB as a stabilizing agent influences the morphology and catalytic activity of carbon-supported CoB catalysts. According to the experimental results, while the effect of CTAB significantly increased the hydrogen production activities of the catalysts up to a certain CTAB (100 µL) concentration, it caused a serious decrease in the hydrogen production rate at higher concentrations. As a result of XRD analysis, it was observed that the addition of CTAB did not affect the crystal structure of the catalysts. As reported in the literature, CoB catalysts maintained their amorphous structure, and therefore, no diffraction peaks were observed in the XRD spectra. When the UV–vis spectrum is examined, the absorbance peak value in the UV region increases linearly with the addition of CTAB. The synthesized catalyst (CoB/C-100CTAB) is used in the hydrolysis of $NaBH_4$, achieving a hydrogen generation rate of 37.34 L_{H2}/min*$g_{catalyst}$, which is notably higher than that of the pre-modified Co—B catalyst. The optimal fuel composition for the CoB/C-CTAB100 catalyst has been determined to be 5 wt% $NaBH_4$ combined with 5 wt% NaOH. As a result of hydrolysis tests carried out at different temperatures, the Arrhenius plot was drawn for the CoB/C-100CTAB catalyst, and the activation energy of the catalyst was calculated as 56 kJ.mol^{-1} by the Arrhenius equation. In the reusability tests, as a result of the 5th cycle, the catalyst lost 40% of its initial activity. The durability test curve given for the CoB/C-100CTAB catalyst shows a parabolic approach. The catalyst surfaces become significantly blocked by metaborates, which are produced as reaction by-products after using the initial 10 mL of fuel. This leads to a considerable drop in catalyst performance. It is believed that this sharp decline in the first test is caused by the metaborates being absorbed into the pores of the carbon support material through capillary action, which slows down the diffusion of BH_4^- ions to the catalyst surface.

Acknowledgments

This research was supported by GreenKnowTech R&D and Consultancy Services. The authors thank GreenKnowTech R&D and Consultancy Services for its support, technical assistance, and access to research facilities, which contributed to the completion of this study.

Conflict of Interests

The authors declare that there are no conflicts of interest regarding the publication of this paper, whether financial, professional, or personal in nature.

Data Availability Statement

Research data are not shared.

Keywords: Cobalt-boride catalysts · Cyclohexyl trimethyl ammonium bromide (CTAB) · Hydrogen generation · Sodium borohydride · Surfactant

[1] R. York, S. E. Bell, *Energy Res. Soc. Sci.* **2019**, *51*, 40–43.
[2] J. E. House, K. A. House, *Descriptive Inorganic Chemistry*, 3rd ed., M. A. Waltham, Academic Press, USA, **2015**.
[3] N. R. J. Hynes, R. Sankaranarayanan, P. S. Kannan, A. Khan, A. A. P. Khan, A. M. Asiri, H. Dzudzevic-Cancar in *Solid-State Hydrides for Hydrogen Storage*, Elsevier **2021**, pp. 249–264.
[4] D. Sui, R. Luo, S. Xie, H. Zhang, T. Ma, H. Sun, T.-T. Jia, J. Sun, X. Li, *Chem. Eng. J.* **2024**, *480*, 148007.
[5] H. Chen, H. Wang, C. Li, *Adv. Mater.* **2022**, *34*, 2205723.
[6] H. N. Abdelhamid, *Int. J. Hydrogen Energy* **2021**, *46*, 726–765.
[7] X. Chen, C. Li, M. Grätzel, R. Kostecki, S. S. Mao, *Chem. Soc. Rev.* **2012**, *41*, 7909.
[8] K. Suárez-Alcántara, J. R. Tena-Garcia, R. Guerrero-Ortiz, *Materials* **2019**, *12*, 2724.
[9] H. Cao, Y. Zhang, J. Wang, Z. Xiong, G. Wu, P. Chen, *Prog. Nat. Sci.: Mater. Int.* **2012**, *22*, 550–560.

© 2025 Wiley-VCH GmbH

23656549, 2025, 30, Downloaded from https://chemistry-europe.onlinelibrary.wiley.com/doi/10.1002/slct.202502538 by Yildiz Teknik University, Wiley Online Library on [06/08/2025]. See the Terms and Conditions (https://onlinelibrary.wiley.com/terms-and-conditions) on Wiley Online Library for rules of use; OA articles are governed by the applicable Creative Commons License

[10] Y. Nakamori, S. Orimo, *Borohydrides as hydrogen storage materials*, Ed: G. Walker, in Solid–State Hydrogen Storage: Materials and Chemistry, Cambridge, UK: Woodhead Publishing, **2008**, pp. 420–449.
[11] P. Knochel, G. A. Molander, Eds., *Comprehensive organic synthesis*, 2nd ed., Amsterdam, Waltham, MA, USA, Elsevier **2014**.
[12] Ç. Çakanyıldırım, M. Gürü, *J. Fac. Eng. Archit. Gazi Univ.* **2022**, *37*, 423–437.
[13] F. Baydaroglu, E. Özdemir, A. Hasimoglu, *Int. J. Hydrogen Energy* **2014**, *39*, 1516–1522.
[14] D. Rohendi, N. Syarif, E. Wati, *IOP Conf. Ser.: Earth Environ. Sci.* **2019**, *248*, 012008.
[15] Y. Shang, R. Chen, *Energy Fuels* **2006**, *20*, 2142–2148.
[16] O. Netskina, D. Kochubey, I. Prosvirin, S. Malykhin, O. Komova, V. Kanazhevskiy, Y. G. Chukalkin, V. Bobrovskii, D. Kellerman, A. Ishchenko, *Mol. Catal.* **2017**, *441*, 100–108.
[17] F. Lin, A. Zhang, J. Zhang, L. Yang, F. Zhang, R. Li, H. Dong, *Colloids Surf. A* **2021**, *626*, 127033.
[18] B. H. Liu, Q. Li, *Int. J. Hydrogen Energy* **2008**, *33*, 7385–7391.
[19] H. Yu, M. A. Tshimanga, T. L. W. Tshimanga, M. Gao, *ChemPhysChem* **2025**, *26*, e202401104.
[20] F. Li, J. Li, L. Chen, Y. Dong, P. Xie, Q. Li, *Int. J. Hydrogen Energy* **2020**, *45*, 32145–32156.
[21] J. H. Türkcan, H. Elçiçek, O. K. Özdemir, *Int. J. Hydrogen Energy* **2021**, *46*, 7903–7911.
[22] F. O. Baydaroglu, E. Özdemir, A. G. Gürek, *React. Kinet., Mech. Catal.* **2017**, *122*, 575–591.
[23] S. Tiwari, C. Mall, P. P. Solanki, *Surfaces and Interfaces* **2020**, *18*, 100427.
[24] S. A. Hoshyar, H. A. Barzani, Y. Yardım, Z. Şentürk, *Colloids Surf. A* **2021**, *610*, 125916.
[25] J. Newton, J. Preece, N. Rees, S. Horswell, *Phys. Chem. Chem. Phys.* **2014**, *16*, 11435–11446.
[26] C. Kaya, J. H. Özdemir, H. Elçiçek, O. K. Özdemir, G. Kökkülünk, K. Ünlügençoğlu, *Int. J. Hydrogen Energy* **2024**, *51*, 489–503.
[27] M. H. Loghmani, A. F. Shojaei, *Int. J. Hydrogen Energy* **2013**, *38*, 10470–10478.
[28] H. Hu, B. Long, Y. Jiang, S. Sun, I. Lawan, W. Zhou, M. Zhang, L. Wang, F. Zhang, Z. Yuan, *Chem. Res. Chin. Univ.* **2020**, *36*, 1209–1216.
[29] V. Singh, R. Tyagi, *J. Taibah Univ. Sci.* **2015**, *9*, 477–489.
[30] J. Chen, B. Long, H. Hu, Z. Zhong, I. Lawa, F. Zhang, L. Wang, Z. Yuan, *Int. J. Hydrogen Energy* **2022**, *47*, 2976–2991.
[31] S. Gupta, N. Patel, R. Fernandes, D. Kothari, A. Miotello, *Int. J. Hydrogen Energy* **2013**, *38*, 14685–14692.
[32] M. H. Loghmani, A. F. Shojaei, M. Khakzad, *Energy* **2017**, *126*, 830–840.
[33] F. O. Baydaroglu, E. Özdemir, A. G. Gürek, *Int. J. Hydrogen Energy* **2022**, *47*, 9643–9652.
[34] K. S. Al-Thubaiti, Z. Khan, S. A. Al-Thabaiti, *J. Mol. Liq.* **2022**, *355*, 118910.
[35] K. Sağır, H. Elçiçek, O. K. Özdemir, *Int. J. Hydrogen Energy* **2021**, *46*, 5689–5698.
[36] M. Aydin, A. Hasimoglu, O. K. Ozdemir, *Int. J. Hydrogen Energy* **2016**, *41*, 239–248.
[37] S. Hoşgün, E. Z. Hoşgün, *Pamukkale Üniversitesi Mühendislik Bilimleri Dergisi* **2024**, *30*, 87–94.
[38] A. Paksoy, S. F. Kurtoğlu, A. K. Dizaji, Z. Altıntaş, S. Khoshsima, A. Uzun, Ö. Balcı, *Int. J. Hydrogen Energy* **2021**, *46*, 7974–7988.
[39] Z. Zaheer, *Colloids Surf., B* **2009**, *69*, 251–256.
[40] S. Wang, H. Xu, L. Qian, X. Jia, J. Wang, Y. Liu, W. Tang, *J. Solid State Chem.* **2009**, *182*, 1088–1093.
[41] L. Shen, F. Tu, Z. Shang, M. Ma, Y. Xia, Z. Zhao, L. Zhao, Z. Wang, G. Shao, *Int. J. Hydrogen Energy* **2022**, *47*, 15001–15011.
[42] Y. Li, X. Gao, X. Iv, Y. Duan, D. Sui, W. Chang, Y. Yang, *ChemCatChem* **2024**, *16*, e202401271.
[43] C.-C. Yang, M.-S. Chen, Y.-W. Chen, *Int. J. Hydrogen Energy* **2011**, *36*, 1418–1423.
[44] C. Wu, F. Wu, Y. Bai, B. Yi, H. Zhang, *Mater. Lett.* **2005**, *59*, 1748–1751.
[45] J. H. Özdemir, B. Aktaş, H. Elçiçek, O. K. Özdemir, Material characterization. In Reference Module in Earth Systems and Environmental Sciences, Elsevier, **2024**.
[46] C. Wu, Y. Tang, A. Zou, J. Li, H. Meng, F. Gao, J. Wu, X. Wang, *DeCarbon* **2025**, *8*, 100108.
[47] A. Kytsya, V. Berezovets, Y. Verbovytskyy, L. Bazylyak, V. Kordan, I. Zavaliy, V. Yartys, *J. Alloys Compd.* **2022**, *908*, 164484.
[48] L. Ai, X. Liu, J. Jiang, *J. Alloys Compd.* **2015**, *625*, 164–170.
[49] Z. Cui, Y. Guo, J. Ma, *Int. J. Hydrogen Energy* **2016**, *41*, 1592–1599.
[50] F. Li, Q. Li, H. Kim, *Chem. Eng. J.* **2012**, *210*, 316–324.
[51] J. Zhao, H. Ma, J. Chen, *Int. J. Hydrogen Energy* **2007**, *32*, 4711–4716.
[52] S. Li, S. Qiu, Y. S. Chua, Y. Xia, Y. Zou, F. Xu, L. Sun, H. Chu, *Mater. Chem. Phys.* **2024**, *319*, 129399.
[53] E. Özdemir, *Int. J. Hydrogen Energy* **2015**, *40*, 14045–14051.
[54] F. Li, J. Li, L. Chen, Y. Dong, P. Xie, Q. Li, *J. Taiwan Inst. Chem. Eng.* **2021**, *122*, 148–156.
[55] L. Shi, W. Xie, Z. Jian, X. Liao, Y. Wang, *Int. J. Hydrogen Energy* **2019**, *44*, 17954–17962.
[56] J. Shen, D. Xu, J. Ji, Q. Zhang, X. Fan, *Int. J. Hydrogen Energy* **2023**, *48*, 1001–1010.
[57] Y.-C. Lu, M.-S. Chen, Y.-W. Chen, *Int. J. Hydrogen Energy* **2012**, *37*, 4254–4258.
[58] Y. Wei, R. Wang, L. Meng, Y. Wang, G. Li, S. Xin, X. Zhao, K. Zhang, *Int. J. Hydrogen Energy* **2017**, *42*, 9945–9951.
[59] C. Peng, T. Li, Y. Zou, C. Xiang, F. Xu, J. Zhang, L. Sun, *Int. J. Hydrogen Energy* **2021**, *46*, 666–675.
[60] J.-H. Wee, *J. Power Sources* **2006**, *155*, 329–339.
[61] Y. Bu, J. Liu, H. Chu, S. Wei, Q. Yin, L. Kang, X. Luo, L. Sun, F. Xu, P. Huang, *Nanomaterials* **2021**, *11*, 3259.

Manuscript received: April 28, 2025

© 2025 Wiley-VCH GmbH

23656549, 2025, 30, Downloaded from https://chemistry-europe.onlinelibrary.wiley.com/doi/10.1002/slct.202502538 by Yildiz Teknik University, Wiley Online Library on [06/08/2025]. See the Terms and Conditions (https://onlinelibrary.wiley.com/terms-and-conditions) on Wiley Online Library for rules of use; OA articles are governed by the applicable Creative Commons License